Scientific
Research
Publishing

Numerical Study of Axial Magnetic Effects on a Turbulent Thermal Plasma Jet for Nanopowder Production Using 3D Time-Dependent Simulation*

Masaya Shigeta

Joining and Welding Research Institute, Osaka University, Ibaraki-shi, Japan
Email: shigeta@jwri.osaka-u.ac.jp

Abstract

3D time-dependent simulations are performed using a computational method suitable for thermal plasma flows to capture a turbulent field induced by a thermal plasma jet and steep gradients in nanopowder distributions. A mathematical model with a simple form is developed to describe effectively simultaneous processes of growth and transport of nanopowder in/around a thermal plasma flow. This growth-transport model obtains the spatial distributions of the number density and mean diameter of nanopowder with a lower computational cost. The results show that an argon thermal plasma jet induces multi-scale vortices even far from itself. A double-layer structure of high-temperature thicker vortex rings surrounded by low-temperature thinner vortex rings is generated in the upstream region. As the vortex rings flow downstream, the high-temperature thicker vortex rings deform largely whereas the low-temperature thinner vortex rings break up into smaller vortices. Nanopowder is generated at the fringe of plasma and transported widely outside the plasma region. The nanopowder grows up collectively by coagulation decreasing particle number as well as homogeneous nucleation and heterogeneous condensation. When a uniform magnetic field is applied in the axial direction, a longer and straighter thermal plasma jet is obtained because of Lorentz force and Joule heating. Larger nanopowder is produced around the plasma because turbulent diffusions of silicon vapor and nanoparticles by vortices are suppressed as well.

Keywords

Thermal Plasma, Nanopowder, Turbulence, Magnetic Field, Flow Control, Simulation

---

*A part of this work was presented at 14th International Conference Fluid Dynamics (ICFD14) in Sendai, 1-3 Nov. 2017.

1. Introduction

Thermal plasmas have been expected as a promising tool for high-speed production of nanopowder because thermal plasmas offer a very-high-temperature field with steep gradients at their fringes where many small nanoparticles are generated rapidly from the material vapor [1]. The fringe of a thermal plasma flow generates vortices by fluid-dynamic instability and the vortices form a complex turbulent flow as revealed experimentally by Pfender *et al.* [2]. The nanopowder grows up and is transported with the turbulent vortices. These simultaneous processes determine the profile of the nanopowder. Meanwhile, an experiment demonstrated that a magnetic field whose direction is the same as the plasma's main flow significantly pinches and concentrates the plasma to the central axis [3]. This fact suggests a possibility that nanopowder production can be controlled through a plasma flow control by applying a magnetic field.

Concerning these backgrounds, here are four problems as follows.

- Simultaneous growth and transport of nanopowder produced by a thermal plasma flow are still poorly understood because it is difficult to investigate them experimentally due to technological limitations.
- Theoretical and computational studies will be powerful approaches. However, after the experiment by Pfender *et al.* [2] in 1991, there has been no report of successful simulation of a turbulent thermal plasma jet having multi-scale vortices in spite of great efforts by several groups [4] [5] [6] [7]. (Most of their works focused on plasma generation inside the nozzle.)
- Up to now, simultaneous growth and transport of nanopowder in/around thermal plasma flows have been simulated only under 2D steady conditions which are oversimplified assumptions [8]-[13]. In nature, nanopowder's growth and transport as well as turbulent plasma flows should be 3D and time-dependent.
- A magnetic pinch effect on a thermal plasma jet has not been studied from the viewpoint of turbulent vortices using 3D time-dependent simulation. That effect on nanopowder production is still unknown as well.

To break through these problems, this study performs 3D time-dependent simulations using a computational method suitable for thermal plasma flows [14] to capture a turbulent field induced by a thermal plasma jet and simultaneous processes of nanopowder's growth and transport. The simulations reveal the effects of an axial magnetic field on the plasma jet and the produced nanopowder.

2. Governing Equations

2.1. Thermal Plasma Jet

Thermal plasma which is generated under atmospheric pressure is described by the thermofluid approximation with several typical assumptions: 1) the entire fluid region including plasma and non-ionized gas is in a local thermodynamic equilibrium state, 2) the plasma is optically thin, and 3) buoyancy due to density

variation is negligible. The governing equations are given as the conservations of mass, momentum and energy:

$$\frac{\partial \rho}{\partial t} + \nabla \cdot (\rho \boldsymbol{u}) = 0 \tag{1}$$

$$\frac{\partial (\rho \boldsymbol{u})}{\partial t} + \nabla \cdot (\rho \boldsymbol{u}\boldsymbol{u}) = -\nabla p + \nabla \cdot \left\{ \eta \left[(\nabla \boldsymbol{u}) + (\nabla \boldsymbol{u})^{tr} - \frac{2}{3}(\nabla \cdot \boldsymbol{u})\boldsymbol{U} \right] \right\} + \boldsymbol{J} \times \boldsymbol{B} \tag{2}$$

$$\frac{\partial (\rho h)}{\partial t} + \nabla \cdot (\rho \boldsymbol{u} h) = \nabla \cdot \left(\frac{\lambda}{C} \nabla h \right) + \frac{\partial p}{\partial t} + \boldsymbol{u} \cdot \nabla p - q_{rad} + q_{con} + \Phi + \frac{|\boldsymbol{J}|^2}{\sigma} \tag{3}$$

where ρ is the density of fluid, t is the time, $\boldsymbol{u}$ is the velocity vector, p is the pressure, η is the viscosity, $\boldsymbol{U}$ is the unit matrix, $\boldsymbol{B}$ is the magnetic flux density vector, h is the enthalpy, λ is the thermal conductivity, C is the specific heat at constant pressure, q_{rad} is the radiation loss, q_{con} is the heat generation due to condensation, Φ is the viscous dissipation, and σ is the electrical conductivity. The superscript tr means transposition. The momentum exchange at nanopowder generation is negligible because the mass flow rate of raw material is small in typical conditions of thermal plasma processing. The terms $\boldsymbol{J} \times \boldsymbol{B}$ and $|\boldsymbol{J}|^2 / \sigma$ are the Lorentz force and the Joule heating which are electromagnetic effects. $\boldsymbol{J}$ is the electric current density vector which is given from the generalized Ohm's law as

$$\boldsymbol{J} = \sigma (\boldsymbol{E} + \boldsymbol{u} \times \boldsymbol{B}) \tag{4}$$

since thermal plasma is regarded as a collision-dominated plasma. $\boldsymbol{E}$ is the electric field vector.

2.2. Nanopowder Growth and Transport

In engineering time- and spatial-scales, the aerosol dynamics approach effectively describes the growth and transport processes of nanopowder produced by thermal plasma with several assumptions: 1) nanopowder consists of spherical nanoparticles, 2) electric charge effects are neglected, 3) nanoparticle temperature is identical to the fluid temperature, and 4) material vapor is treated as an ideal gas. Extending the previous model [15] for nanopowder growth through homogeneous nucleation, heterogeneous condensation and coagulation between nanoparticles, the governing equations that also express the nanopowder's transport by convection, diffusion and thermophoresis are written as

$$\begin{aligned} &\rho \frac{\partial}{\partial t}\left(\frac{n_p}{\rho}\right) + \rho \boldsymbol{u} \cdot \nabla \left(\frac{n_p}{\rho}\right) \\ &= \nabla \cdot \left[\rho D_p \nabla \left(\frac{n_p}{\rho}\right) \right] + I - 2\sqrt{2}\beta_0 n_p^{11/6} f^{1/6} - \nabla \cdot \left(K_{th}\eta \frac{n_p}{\rho} \nabla \ln T \right) \end{aligned} \tag{5}$$

$$\begin{aligned} &\rho \frac{\partial}{\partial t}\left(\frac{f}{\rho}\right) + \rho \boldsymbol{u} \cdot \nabla \left(\frac{f}{\rho}\right) \\ &= \nabla \cdot \left[\rho D_p \nabla \left(\frac{f}{\rho}\right) \right] + I g_c + \beta_0 (n_v - n_s) n_p^{1/3} f^{2/3} - \nabla \cdot \left(K_{th}\eta \frac{f}{\rho} \nabla \ln T \right) \end{aligned} \tag{6}$$

$$\rho \frac{\partial}{\partial t}\left(\frac{n_v}{\rho}\right) + \rho \boldsymbol{u} \cdot \nabla\left(\frac{n_v}{\rho}\right) = \nabla \cdot \left[\rho D_v \nabla\left(\frac{n_v}{\rho}\right)\right] - I g_c - \beta_0 \left(n_v - n_s\right) n_p^{1/3} f^{2/3} \quad (7)$$

where n is the number density, D is the diffusion coefficient, and T is the temperature. The subscripts p, v, and s denote particle, vapor, and saturated state, respectively. The variable f is defined as $f = n_p g$. D_p is the diffusion coefficient of nanoparticles derived from [16] as

$$D_p = \frac{k_B T}{3\pi \eta d_v}\left(g^{-1/3} + 3.314\frac{l}{d_v}g^{-2/3}\right) \quad (8)$$

where k_B is the Boltzmann constant, d is the diameter, g is the average monomer number in a nanoparticle, l is the mean free path. D_v is the diffusion coefficient of material vapor obtained from the molecular theory by Hirschfelder *et al.* [17]. I is the homogeneous nucleation rate and g_c is the number of monomers composing a nanoparticle in a critical state, which are estimated by the modified self-consistent nucleation theory by Girshick *et al.* [18]. β_0 is the parameter related to collision frequency given as [15]

$$\beta_0 = \left(\frac{3v_v}{4\pi}\right)^{1/6}\sqrt{\frac{6k_B T v_v}{m_v}} \quad (9)$$

where v is the volume and m is the mass. K_{th} is the thermophoresis coefficient [19]. The third term in the right hand side of Equation (5) denotes the contribution of coagulation among nanoparticles. The third terms in the right hand sides of Equation (6) and Equation (7) mean the contribution of heterogeneous condensation. Therefore, the heat generation due to condensation in Equation (3) is given by

$$q_{con} = m_v H_v \beta_0 \left(n_v - n_s\right) n_p^{1/3} f^{2/3} \quad (10)$$

where H_v is the latent heat of vaporization.

This growth-transport model obtains the spatial distributions of the number density n_p and the mean diameter $\langle d_p \rangle = d_v \left(f/n_p\right)^{1/3}$ of nanoparticles in spite of its much simpler mathematical form than the often-used model which is known as the method of moment [8] [9] [10] [11] [12], [16]. By virtue of its simplicity, the computation can be performed with a lower computational cost than other models [8]-[13], [16].

3. Computational Methods and Conditions

3.1. Computational Methods

The present computation is addressed by an approach of large eddy simulation (LES). For LES, the governing equations are typically transformed using the filtering operations. The turbulent features at the sub-grid scale (SGS) are treated by the coherent structure model [20], [21] because thermal plasma simulation requires capability of expressing both laminar and turbulent states [14]. Turbulent diffusion of nanopowder at the SGS is given as the same manner as that of chemical species.

To solve the governing equations, a computational method "*Method-III*" proposed in [14] is used. This method can express multi-scale turbulent vortices and a nanopowder distribution with steep gradients in/around a thermal plasma flow which has large variations of density and transport properties.

3.2. Computational Conditions

Figure 1 shows a schematic illustration of the computation domain. A non-transferred argon thermal plasma jet is ejected from a circular nozzle with the diameter of 8.0 mm. At the nozzle exit, the plasma jet has steady profiles of velocity with the maximum 400 m/s and temperature with the maximum 12,000 K presented as Figure 2. These conditions are obtained from the approximated curves [14] with the experiment data [2]. Silicon vapor is supplied at 0.1 g/min with the plasma jet. When a magnetic field is applied, a magnetic flux density of 1.0 T is given in x direction uniformly in the whole domain. Because this study treats plasma flows outside the nozzle, the electric field to generate plasma inside the nozzle can be neglected; that is, $E = 0$ in the computational domain.
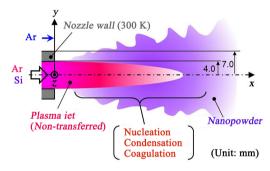

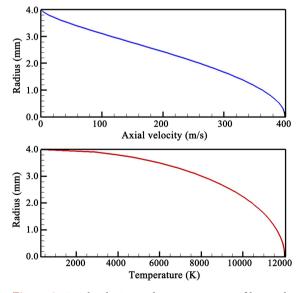**Figure 1.** Schematic illustration of nanopowder production by a thermal plasma jet.

Figure 2. Axial velocity and temperature profiles at the nozzle exit.

The geometries of the domain are (x, y, z) = (0.0 - 255.8 mm, −51.2 - 51.1 mm, −51.2 - 51.1 mm). For the downstream outlet boundary, the unsteady outflow conditions based on mass conservation considering variable density [22] are adopted. Periodic conditions are set on the boundaries in y and z directions. Computations are performed using a Cartesian staggered grid system with the uniform spatial interval of $\Delta x = \Delta y = \Delta z$ = 0.1 mm and the time increment of Δt = 0.1 ms on a supercomputer SX-ACE (NEC) at Tohoku University, Japan.

The thermodynamic and transport properties of argon thermal plasma and non-ionized argon gas exhibit large variations with one or two orders of magnitude. This study takes account of those characteristics by implementing the temperature-dependent data [23]. The material properties of silicon are obtained from the database [24].

4. Results and Discussion

Figure 3(a) and Figure 3(b) show the snapshots of isothermal surfaces of 6000 K and 9000 K without and with a uniform axial magnetic field, respectively. It is noted that the region near the jet nozzle (x, y, z) = (0.0 - 125.0 mm, −31.5 - 31.5 mm, −31.5 - 31.5 mm) is presented. t_0 is an arbitrary time after the flow field becomes quasi-periodic. With the magnetic field in Figure 3(b), the plasma jet core represented by the 9000 K isosurface has a longer and straighter shape, compared to that without the magnetic filed in Figure 3(a). These results agree with the experiment [3]. Figure 4 depicts the time evolutions of the axial tip positions of the jet cores for both conditions. The jet cores extend and break up periodically, which results in the zigzag profiles in Figure 4. The broken tips flow downstream and then disappear with decrease in temperature. Figure 4 tells quantitatively that the plasma jet is longer when the magnetic field is applied. One of the reasons for this elongation is the induced Joule heating. The velocity components perpendicular to the magnetic field induce electric current as described in Equation (4). The induced electric current produces the Joule heating by itself as given in Equation (3). Without the magnetic field, the extension-breakup process occurs more irregularly. This is related to wavy shapes of the 6000 K isosurfaces in Figure 3(a).

Figure 5(a) and Figure 5(b) show the snapshots of velocity vectors on y-z cross-sections of every 24.0 mm at the same moments as Figure 3(a) and Figure 3(b). Correspondingly, the high speed plasma jet is sustained longer with the magnetic field. To understand a complicated flow field in turbulence, it is convenient to visualize the vortices. Figure 6(a) and Figure 6(b) show the snapshots of the vortex structures. These coherent structures of vortices can be extracted from the velocity data by a vortex identification method which is called "*Q-criterion*" [25]. Here, the vortices are presented by the isosurfaces of the second invariant of the velocity gradient tensor of the value 0.25 s^{-2} which was normalized by the mean velocity of 160 m/s and the diameter of 8.0 mm at the

nozzle exit. Many vortices are generated even far from the plasma jet cores. These visualized vortex structures are similar to the Schlieren photograph by Pfender *et al.* [2]. Large vortices have higher temperatures whereas small vortices have lower temperatures as predicted on the basis of Kolmogorov theory [14], [26]. With the magnetic field in Figure 6(b), the structure of vortices is less complex because the magnetic field induces Lorentz force to suppress velocity
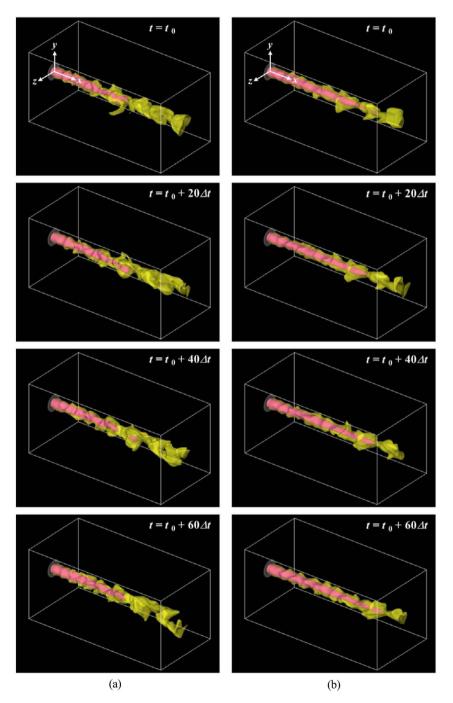

Figure 3. Snapshots of thermal plasma jets represented by isothermal surfaces of 6000 K (yellow) and 9000 K (pink). (a) Without magnetic field (0.0 T); (b) With magnetic field (1.0 T).
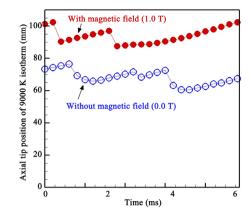
Figure 4. Time evolutions of axial tip positions of thermal plasma jets.
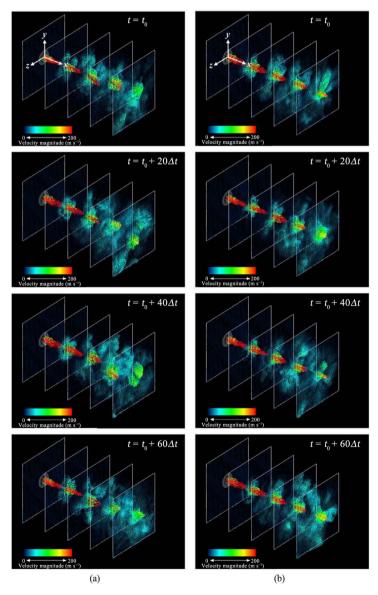

(a)

(b)

Figure 5. Snapshots of velocity vectors on *y-z* cross-sections of every 24.0 mm. (a) Without magnetic field (0.0 T); (b) With magnetic field (1.0 T).
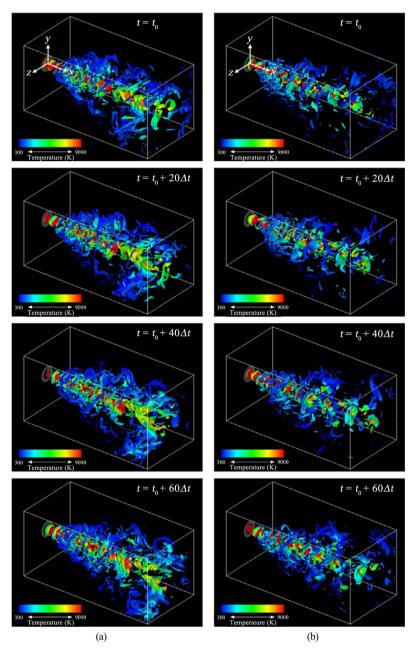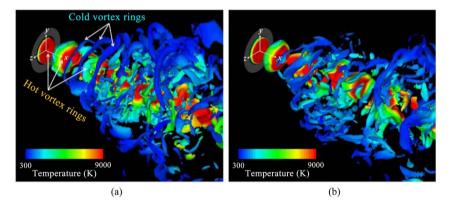
Figure 6. Snapshots of vortex structures represented by the second invariant of the velocity gradient tensor. (a) Without magnetic field (0.0 T); (b) With magnetic field (1.0 T).

fluctuation causing vortices. The velocity fluctuations also induce electric current. The electric current components perpendicular to the magnetic field produce the Lorentz force in the direction perpendicular to both the electric current and the magnetic field. This direction of the Lorentz force is the opposite direction to the velocity fluctuation. In consequent, the velocity fluctuations are suppressed as described in Equation (2). **Figure 7(a)** and **Figure 7(b)** present the magnified snapshots. **Figure 7(a)** clearly shows a double-layer structure of high-temperature thicker vortex rings surrounded by low-temperature thinner

vortex rings in the upstream region. As they flow downstream, the high-temperature thicker vortex rings deform largely whereas the low-temperature thinner vortex rings break up into smaller vortices. **Figure 7(b)** shows a similar but less complex vortex structure because of the suppression effect by the magnetic field.

Figure 8(a) and **Figure 8(b)** depict the standard deviations of vorticity magnitude fluctuation on the central cross-sections without and with the magnetic field, respectively. These standard deviations were obtained from the quasi-periodic data sets during 12.8 ms. The frequency of the fluctuation ranged from 588 Hz to 714 Hz. This period included 8 oscillations. This number is not always sufficient for experimental studies. On the other hand, for a computational study with higher reproducibility, it is acceptable for qualitative estimation and discussion. For both conditions, the regions outside the plasma jets have large fluctuations due to vortices, while the plasma core regions have negligibly small fluctuation because high-temperature plasmas offer much larger viscosities. When the magnetic field is applied, the fluctuation is suppressed remarkably. This means that the magnetic field decreases vortices which transport energy and mix the field effectively. In consequence, that plasma jet in the magnetic field is straighter and longer as shown in **Figure 3** and **Figure 4**.
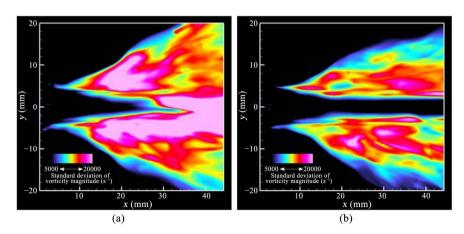

(a)   (b)

Figure 7. Magnified snaphots of vortex structures. (a) Without magnetic field (0.0 T); (b) With magnetic field (1.0 T).

(a)   (b)

Figure 8. Standard deviations of vorticity magnitude fluctuation on central cross-sections ($z = 0$). (a) Without magnetic field (0.0 T); (b) With magnetic field (1.0 T).

Figure 9 shows the snapshots of the nanopowder distributions without and with the magnetic field, respectively. The distributions are expressed by the isosurfaces of the particle number density of 2.0×10^{18} m^{-3}, 1.0×10^{19} m^{-3}, and 5.0×10^{19} m^{-3}. Figure 10 illustrates the mean diameter distributions of the nanopowder on the isosurface of the particle number density of 3.2×10^{18} m^{-3}.
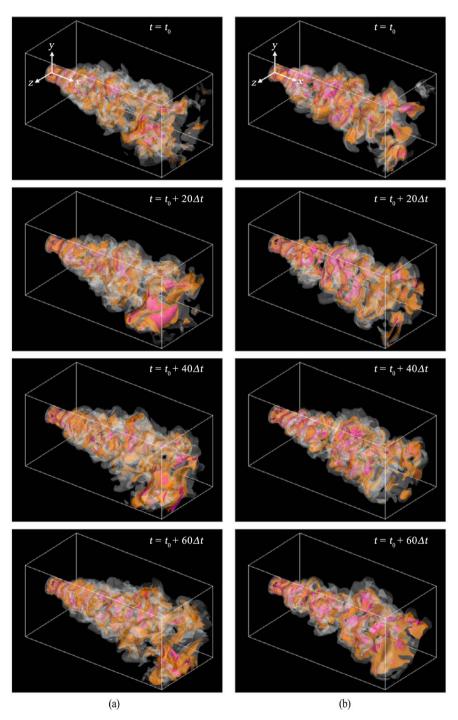

Figure 9. Snapshots of nanopwder distributions expressed by isosurfaces of particle number density of 2.0×10^{18} m^{-3}, 1.0×10^{19} m^{-3}, and 5.0×10^{19} m^{-3}. (a) Without magnetic field (0.0 T); (b) With magnetic field (1.0 T).
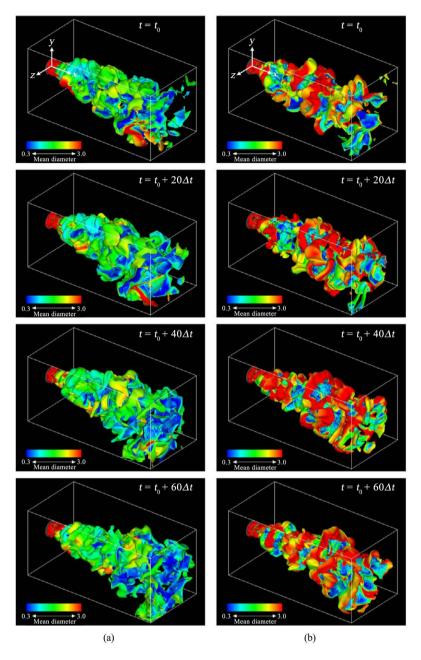
Figure 10. Snapshots of mean diameter distributions of nanopowder on isosurface of particle number density of 3.2×10^{18} m^{-3}. (a) Without magnetic field (0.0 T); (b) With magnetic field (1.0 T).

Figure 11 and **Figure 12** present the corresponding distributions of number density and mean diameter on the cross-sections of $y = 0$ ($z > 0$) and $z = 0$ ($y > 0$). The material vapor in the plasma jet is transported by convection and diffusion. At the plasma fringe with lower temperature, the material vapor becomes supersaturated and changes its phase into nanopowder by homogeneous nucleation and heterogeneous condensation. Because nanopowder collectively grows up and diffuses outside the plasma region, nanopowder distributes widely in the field. The larger size regions in **Figure 12** coincide with smaller number density

regions in **Figure 11**. This result indicates that simultaneous coagulation decreasing particle number plays an important role for nanopowder growth as well. When the magnetic field is applied, the distribution exhibits a thinner shape because of the suppression effect on the turbulent field. In the less turbulent field resulted from the magnetic field, the material vapor is not transported outward very much but stay near the plasma's fringe. As a result, the nanopowder has larger particle sizes due to more significant condensation. This tendency coincides with a result obtained by a different computational work [13].
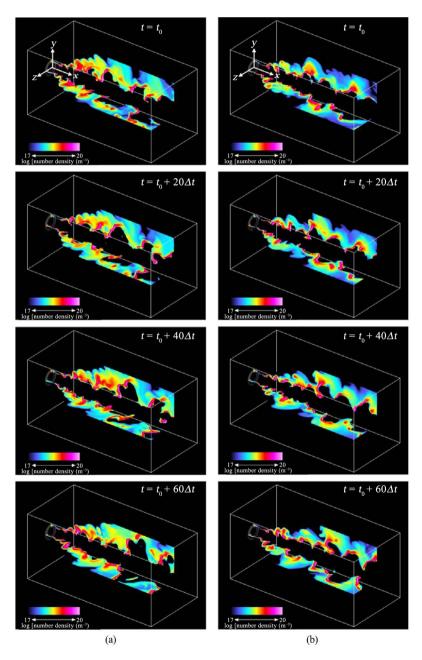

(a)   (b)

Figure 11. Snapshots of number density distributions of nanopowder on cross-sections of $y = 0$ ($z > 0$) and $z = 0$ ($y > 0$). (a) Without magnetic field (0.0 T); (b) With magnetic field (1.0 T).

Figure 12. Snapshots of mean diameter distributions of nanopowder on cross-sections of $y = 0$ ($z > 0$) and $z = 0$ ($y > 0$). (a) Without magnetic field (0.0 T); (b) With magnetic field (1.0 T).
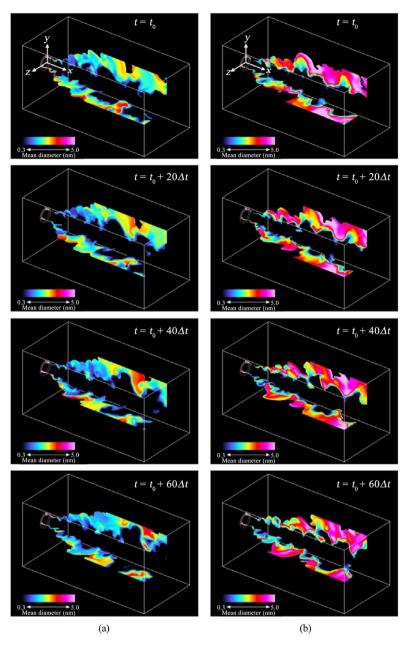
5. Conclusions

3D time-dependent simulations were performed using a computational method suitable for thermal plasma flows to capture a turbulent field induced by a thermal plasma jet and steep gradients in nanopowder distributions. A mathematical model with a simple form was developed to describe effectively simultaneous processes of growth and transport of nanopowder in/around a thermal plasma flow. This growth-transport model obtained the spatial distributions of the number density and mean diameter of nanopowder with a lower computational

cost. The major findings are enumerated as follows.

- An argon thermal plasma jet induces multi-scale vortices even far from itself. A double-layer structure of high-temperature thicker vortex rings surrounded by low-temperature thinner vortex rings is generated in the upstream region. As the vortex rings flow downstream, the high-temperature thicker vortex rings deform largely whereas the low-temperature thinner vortex rings break up into smaller vortices.

- Nanopowder is generated at the fringe of plasma and transported widely outside the plasma region. The regions where the nanopowder has larger size coincide with the regions where the nanopowder exhibits smaller number density. This result indicates that nanopowder grows up significantly by coagulation decreasing particle number as well as homogeneous nucleation and heterogeneous condensation.

- When a uniform magnetic field is applied in the axial direction, a longer and straighter thermal plasma jet is obtained because the induced Lorentz force suppresses turbulent vortices and the Joule heating is also generated in the plasma. Larger nanopowder is produced around the plasma because turbulent diffusions of silicon vapor and nanoparticles by vortices are suppressed as well.

Acknowledgements

References

[1] Shigeta, M. and Murphy, A.B. (2011) Thermal Plasmas for Nanofabrication. *Journal of Physics D: Applied Physics*, **44**, Article ID: 174025, 16 p.

[2] Pfender, E., Fincke, J. and Spores, R. (1991) Entrainment of Cold Gas into Thermal Plasma Jets. *Plasma Chemistry and Plasma Processing*, **11**, 529-543.
https://doi.org/10.1007/BF01447164

[3] Sato, T., Shigeta, M., Kato, D. and Nishiyama, H. (2001) Mixing and Magnetic Effects on a Nonequilibrium Argon Plasma Jet. *International Journal of Thermal Sciences*, **40**, 273-278. https://doi.org/10.1016/S1290-0729(00)01217-5

[4] Colombo, V., Concetti, A. and Ghedini, E. (2007) Time Dependent 3D Large Eddy Simulation of a DC Non-Transferred Arc Plasma Spraying Torch with Particle Injections. *Proceedings of the* 16*th IEEE International Pulsed Power Conference*, Albuquerque, 17-22 June 2007, 1565-1568.
https://doi.org/10.1109/PPPS.2007.4652486

[5] Marchand, C., Chazelas, C., Mariaux, G. and Vardelle, A. (2007) Liquid Precursor Plasma Spraying: Modeling the Interactions between the Transient Plasma Jet and

the Droplets. *Journal of Thermal Spray Technology*, **16**, 705-712.
https://doi.org/10.1007/s11666-007-9112-x

[6]   Meillot, E., Vincent, S., Caruyer, C., Damiani, D. and Caltagirone, J.P. (2013) Modelling the Interactions between a Thermal Plasma Flow and a Continuous Liquid Jet in a Suspension Spraying Process. *Journal of Physics D: Applied Physics*, **46**, Article ID: 224017, 11 p.

[7]   Trelles, J.P. and Modirkhazeni, S.M. (2014) Variational Multiscale Method for Nonequilibrium Plasma Flows. *Computer Methods in Applied Mechanics and Engineering*, **282**, 87-131. https://doi.org/10.1016/j.cma.2014.09.001

[8]   Girshick, S.L, Chiu, C.-P., Muno, R., Yu, W., Yang, L., Singh, S.K. and McMurry, P.H (1993) Thermal Plasma Synthesis of Ultrafine Iron Particles. *Journal of Aerosol Science*, **24**, 367-382. https://doi.org/10.1016/0021-8502(93)90009-X

[9]   Bilodeau, J.F. and Proulx, P. (1996) A Mathematical Model for Ultrafine Iron Powder Growth in Thermal Plasma. *Aerosol Science and Technology*, **24**, 175-189. https://doi.org/10.1080/02786829608965362

[10] Désilets, M., Bilodeau, J.F. and Proulx, P. (1997) Modelling of the Reactive Synthesis of Ultra-Fine Powders in a Thermal Plasma Reactor. *Journal of Physics D: Applied Physics*, **30**, 1951-1960. https://doi.org/10.1088/0022-3727/30/13/018

[11] Shigeta, M. and Watanabe, T. (2008) Numerical Investigation of Cooling Effect on Platinum Nanoparticle Formation in Inductively Coupled Thermal Plasmas. *Journal of Applied Physics*, **103**, Article ID: 074903, 15 p.

[12] Shigeta, M. and Watanabe, T. (2008) Two-Dimensional Analysis of Nanoparticle Formation in Induction Thermal Plasmas with Counterflow Cooling. *Thin Solid Films*, **516**, 4415-4422. https://doi.org/10.1016/j.tsf.2007.10.022

[13] Colombo, V., Ghedini, E., Gherardi, M., Sanibondi, P. and Shigeta, M. (2012) A Two-Dimensional Nodal Model with Turbulent Effects for the Synthesis of Si Nano-Particles by Inductively Coupled Thermal Plasmas. *Plasma Sources Science and Technology*, **21**, Article ID: 025001, 12 p.

[14] Shigeta, M. (2016) Turbulence Modelling of Thermal Plasma Flows. *Journal of Physics D: Applied Physics*, **49**, Article ID: 493001, 18 p.

[15] Nemchinsky, V.A. and Shigeta, M. (2012) Simple Equations to Describe Aerosol Growth. *Modelling and Simulation in Materials Science and Engineering*, **20**, Article ID: 045017, 11 p.

[16] Phanse, G.M. and Pratsinis, S.E. (1989) Theory for Aerosol Generation in Laminar Flow Condensers. *Aerosol Science and Technology*, **11**, 100-119. https://doi.org/10.1080/02786828908959304

[17] Hirschfelder, J.O., Curtiss, C.F. and Bird, R.B. (1964) Molecular Theory of Gases and Liquids. Wiley, New York.

[18] Girshick, S.K., Chiu, P.C. and McMurry, P.H. (1990) Time-Dependent Aerosol Models and Homogeneous Nucleation Rates. *Aerosol Science and Technology*, **13**, 465-477. https://doi.org/10.1080/02786829008959461

[19] Talbot, L., Cheng, R.K., Schefer, R.W. and Willis, D.R. (1979) Thermophoresis of Particles in a Heated Boundary Layer. *Journal of Fluid Mechanics*, **101**, 737-758. https://doi.org/10.1017/S0022112080001905

[20] Kobayashi, H. (2005) The Subgrid-Scale Models Based on Coherent Structures for Rotating Homogeneous Turbulence and Turbulent Channel Flow. *Physics of Fluids*, **17**, Article ID: 045104.

[21] Kobayashi, H. (2006) Large Eddy Simulation of Magnetohydrodynamic Turbulent

Channel Flows with Local Subgrid-Scale Model Based on Coherent Structures. *Physics of Fluids*, **18**, Article ID: 045107.

[22] Matsushita, Y. (2011) Outflow Boundary Condition in the Finite Volume Method for Unsteady-State Fluid Flow Computation with Variable Density. *Computational Thermal Sciences*, **3**, 531-537.
https://doi.org/10.1615/ComputThermalScien.2012003330

[23] Boulos, M.I., Fauchais, P. and Pfender, E. (1994) Thermal Plasmas Fundamentals and Applications. Volume 1, Plenum Press, New York.

[24] Japan Institute of Metals (1993) Metal Data Book. Maruzen, Tokyo.

[25] Hunt, J.C.R., Wray, A.A. and Moin, P. (1988) Eddies, Streams, and Convergence Zones in Turbulent Flows. Center for Turbulence Research, 193-208.
https://web.stanford.edu/group/ctr/Summer/201306111537.pdf

[26] Shigeta, M. (2012) Time-Dependent 3-D Simulation of an Argon RF Inductively Coupled Thermal Plasma. *Plasma Sources Science and Technology*, **21**, Article ID: 055029.